J. Fluid Mech. (1982), *vol.* 125, *pp.* 187–202
Printed in Great Britain

Coaxial scattering of Euler-equation translating V-states via contour dynamics

By EDWARD A. OVERMAN AND NORMAN J. ZABUSKY

Institute for Computational Mathematics and Applications, Department of Mathematics and Statistics, University of Pittsburgh, Pittsburgh, PA 15261

(Received 16 February 1982 and in revised form 7 June 1982)

The robustness of localized states that transport energy and mass is assessed by a numerical study of the Euler equation in two space dimensions. The localized states are the translating 'V-states' discovered by Deem & Zabusky. These piecewise-constant dipolar (i.e. oppositely-signed $\pm$ or $\mp$) vorticity regions are steady translating solutions of the Euler equations. A new adaptive contour-dynamical algorithm with curvature-controlled node insertion and removal is used. The evolution of one V-state, subject to a symmetric-plus-asymmetric perturbation is examined and stable (i.e. non-divergent) fluctuations are observed. For scattering interactions, *coaxial* head-on (or $\pm$ on $\mp$) and head-tail (or $\pm$ on $\pm$) arrangements are studied. The temporal variation of contour curvature and perimeter after V-states separate indicate that internal degrees of freedom have been excited. For weak interactions we observe phase shifts and the near recurrence to initial states. When two similar, equal-circulation but unequal-area V-states have a head-on interaction a new asymmetric state is created by contour 'exchange'. There is strong evidence that this is near to a V-state. For strong interactions we observe phase shifts, 'breaking' (filament formation) and, for head–tail interactions, merger of like-signed vorticity regions.

1. Introduction

It is well-known that solitary (nonlinear-dispersive) waves can transport energy over long distances and deposit it in small inhomogeneous spatial regions. Some of these systems can be described by non-dissipative one-space and one-time dimensional equations whose solitary waves are solitons. These systems are 'integrable' and the solitons are preserved through interactions. If small amounts of dissipation are added to some of these systems they become 'near-integrable' and the soliton becomes a slowly decaying solitary entity. However, in many cases the essential features of soliton interactions are preserved. Some aspects of this subject are discussed in the review by Zabusky (1981).

We now ask: Can one find localized steady-state entities in *two space* dimensions that can transport energy and mass? Furthermore, how robust are these entities when interacting with each other? Nuclear physicists have begun to study nonlinear dynamical problems with finite-difference simulations of particle-like entities characterized by 'confinement potentials' (Makhanov 1980; Simonov & Tjon 1980). McWilliams & Zabusky (1982) have examined 'modon' interactions by finite-difference simulations. These modons are steady-state solutions of the geostrophic β-plane equations that have *continuous* distributions of vorticity in localized regions (Flierl *et al.* 1980) and have been associated with the phenomenon of atmospheric 'blocking' (McWilliams 1980).

In the present paper we will apply a contour dynamical algorithm to study the interaction of translating 'V-states', steady-state solutions of the two-dimensional Euler equations (Deem & Zabusky 1978*a*, *b*). These states, discovered by Deem & Zabusky, are localized dipolar (i.e. oppositely signed) *piecewise-constant* vorticity regions. In the contour-dynamics approach we study the evolution of piecewise-constant quantities by following the motion of their boundaries. This contour-integral method employs a Green function for the unbounded domain and does not require an underlying two-dimensional mesh. The present improved algorithm is *adaptive*, and inserts and removes nodes as a function of local curvature. Thus, it can follow accurately the evolution of contours into narrow sheet-like vortex regions. A similar algorithm was used to study the 'merger' of monopolar (i.e. like-signed) vortex regions (Overman & Zabusky 1982).

We will study numerically parameter regions where the interactions lead to either the formation of new nearly-stationary states, the near-recurrence of initial states, or strong deformation and breaking of initial states. In §2 and appendix B we discuss the improved contour dynamical algorithm and diagnostics including the contour curvature. In §3 we discuss the results obtained from various simulations. In §4 we indicate possible directions for future research.

2. Euler equations, translating V-states, contour-dynamical algorithm and diagnostics

The Euler equations in two space dimensions can be written in vorticity–stream-function form as

$$\omega_t + u\omega_x + v\omega_y = 0, \quad \Delta\psi \equiv \psi_{xx} + \psi_{yy} = -\omega, \tag{1a, b}$$

where

$$u = \psi_y, \quad v = -\psi_x. \tag{1c}$$

If the vorticity is composed of a set of piecewise-constant finite-area-vortex regions (or FAVRs), that is, each member of the set is a characteristic function χ_i of magnitude ω_i and boundary ∂D_i, or $\omega(x, y, t) = \Sigma_i \omega_i \chi_i(x, y, t)$, then

$$\psi(x, y) = -(2\pi)^{-1} \sum_i \iint_{\mathbb{R}^2} \omega_i \chi_i G(x-\xi, y-\eta)\, d\xi\, d\eta, \tag{2}$$

where we use the two-dimensional Green function

$$G \equiv \tfrac{1}{2}\log[(x-\xi)^2 + (y-\eta)^2] = \log r, \tag{3}$$

for flow in an unbounded domain. Equation (1*a*) says that every point of the fluid including the boundary is convected with the flow. The evolution equations for boundary points (x, y) is the *area-preserving* mapping

$$(x_t, y_t) \equiv (u(x, y, t), v(x, y, t)) = (2\pi)^{-1} \sum_i \omega_i \int_{\partial D_i} \log r(d\xi, d\eta). \tag{4}$$

We have used Green's theorem to replace the area integral over the domain of χ_i by the line integral over ∂D_i thus reducing the dimension by one.

It is well known that two point (singular) vortices of opposite (i.e. dipolar) circulation $\pm\Gamma$ and separation $2\bar{y}$ translate parallel to the x-axis with speeds

$$V^* = \frac{|\Gamma|}{4\pi\bar{y}}. \tag{5}$$

To find a symmetric doubly-connected FAVR that translates with velocity V parallel to the x-axis, we apply the boundary condition

$$\mathbf{n} \cdot \mathbf{v}_{\text{particle}} = \mathbf{n} \cdot \mathbf{v}_{\text{boundary}}, \tag{6}$$

or

$$\partial_s \psi + V \frac{dy}{ds} = 0. \tag{7}$$

We integrate once to obtain

$$\psi(x, y) + Vy = c_i, \quad (x, y) \in \partial D_i, \tag{8}$$

where the c_i are constants and $i = 1, 2$ corresponds to the contours. ψ is obtained from (2) as a line integral over both contours. Since the location of the boundary is unknown, (7) or (8) are nonlinear integral equations.

The first translating V-state was obtained from a discretized form of (7) by Deem & Zabusky (1978*a*). They can be thought of as a piecewise-constant 'desingularization' of two oppositely-signed point vortices. Using a discretized form of (8), Pierrehumbert (1980) obtained a set of 12 states whose upper half-plane contour lies in the range $y_{\min} \leqslant y \leqslant 1{\cdot}0$ (and $y_{\min} = 0$, the limiting case). He studied their properties, including the variation of V/V^* with $y_{\min}$. For $0{\cdot}01 \leqslant y_{\min} \leqslant 0{\cdot}9$, Wu, Overman & Zabusky (1982) verified the results of Pierrehumbert, as shown in figure 1 and summarized in appendix A. (However, his limiting case is not accurate.) In the scattering simulations described below we use state H (between G and I in figure 1), where $y_{\min} = 0{\cdot}2$.

The contour-dynamics algorithm is obtained by discretizing (4) (Zabusky, Hughes & Roberts 1979), i.e.

$$(\dot{x}_m, \dot{y}_m) = \sum_i \omega_i \sum_{n=1}^{N_i} \Delta u_{m,n;i} (\cos \theta_{n;i}, \sin \theta_{n;i}), \tag{9}$$

where the i-sum is over all the contours. $\Delta u_{m,n;i}$ is given in appendix B along with an algorithm for node insertion and removal to control truncation errors. An Euler-predictor trapezoidal-corrector algorithm is used to solve the ordinary differential equations in (9), and the choice of the time step is also discussed in appendix B.

3. Dynamical evolution of pairs of translating *V*-states

3.1. *Introduction*

In this first study of translating V-state interactions we simplify the parameter space by examining coaxial collisions. The resulting symmetry allows us to reduce the computational load by a factor of 2.

We use two forms of V-state H (see table 2 in appendix A), which we henceforth call V-state no. 1 and V-state no. 2. V-state no. 1 lies in the range $0{\cdot}2 \leqslant y \leqslant 1{\cdot}0$ and always has an upper half-plane vorticity density of $+1{\cdot}0$. To study size effects, V-state no. 2 either lies in the range $0{\cdot}2 \leqslant y \leqslant 1{\cdot}0$ or $0{\cdot}1 \leqslant y \leqslant 0{\cdot}5$ (i.e. it has been scaled down by a factor of two) and has various vorticity densities. Table 1 gives parameters for the cases (*a*)–(*m*) discussed below. This letter designation is also adopted in the figures, e.g. figure 4(*c*) gives results for case (*c*) on figure 4.

3.2. *Diagnostics*

To summarize the interactions we generally give figures composed of panels showing the upper-half-plane contours, where time increases downwards. In some intervals

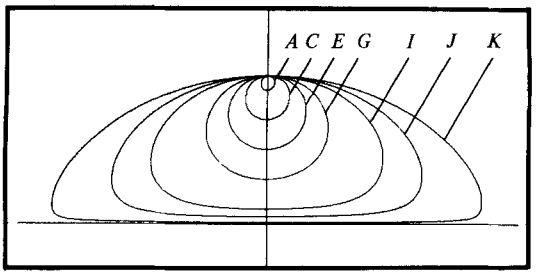

FIGURE 1. Translating V-states of the two-dimensional Euler equations. Only the upper-half-plane contours are shown. The lower-half-plane contours are symmetric.

the panels are equally spaced in time to aid the reader to obtain a space–time feeling for the event. In all cases the spatial scales of all panels on each figure are identical. On separate figures (11 and 12) we give respectively a trajectory diagram $(\bar{x}(t), \bar{y}(t))$ and a 'phase-shift' diagram $(\bar{x}(t), t)$ of the centroids of the upper-half-plane V-state contours. In figures 2, 3 and 8 we also present selected diagnostics like area change $(\Delta A/A)_i$, perimeter change $(\Delta P/P)_i$, total velocity change $(\Delta V/V)_i$ and max|curvature| change $(\Delta\kappa/\kappa)_i$ *vs.* time. The scalar changes are defined as

$$\left(\frac{\Delta q}{q}\right)_i \equiv \left(\frac{q_i(t)}{q_i(0)}\right) - 1,$$

and the total velocity change is defined as

$$\left(\frac{\Delta V}{V}\right)_i \equiv \frac{|\mathbf{V}_i(t)|}{|\mathbf{V}_i(0)|} - 1,$$

where $\mathbf{V}_i$ is the velocity of the centroid of contour i, obtained by a simple difference. The curvature of a contour

$$\kappa(s) = x_s y_{ss} - y_s x_{ss}$$

is computer numerically by differentiating a periodic cubic spline that is fit to the nodes (as described in appendix C of Zabusky & Overman 1982). If contours 'sharpen' and 'break', as observed below, this differentiation can give rise to local small-scale oscillations because the cubic spline has difficulty fitting such distributions. These oscillations do not affect our velocities since the curvature is not used in evaluating $\Delta u_{m,n;i}$ in (9). (See figure 10 for initial and final curvatures of case (*l*).

3.3. *Stability of a translating V-state*

We examine the question of the stability of V-state H to an asymmetric perturbation by the method of detailed numerical simulation. We do *not* assume symmetry about the x-axis, and begin with an initial state constructed as follows.

(i) The upper and lower contours of V-state H are displaced toward the x-axis by 0·05. Hence the smallest distance between the upper and lower contours is 0·3.

(ii) The upper contour $R_+(s)$ is perturbed with a 'third' harmonic. That is, if $\mathbf{R}_+(s)$ is the position as a function of arclength with respect to the centroid, we obtain the perturbed position $\mathbf{R}$ as

$$\mathbf{R}(s) = \mathbf{R}_+(s) + 0{\cdot}01 \cos\left(\frac{6\pi s}{P_+}\right)\mathbf{e}_n(s),$$

where $\mathbf{e}_n(s)$ is the outward normal to the unperturbed contour, and P_+ is the perimeter of the unperturbed contour.

Case	ω_2	Γ_2/Γ_1	Γ_2	A_2/A_1	$\bar{y}_2/\bar{y}_1$	$\bar{x}_c(0)$	V_2	V_2/V_1	Run
(*a*)	−4·0	−1·0	−0·6846	$\frac{1}{4}$	$\frac{1}{2}$	4	−0·176	−2·0	XS 2S02
(*b*)	−2·0	−0·5	−0·3422	$\frac{1}{4}$	$\frac{1}{2}$	8	−0·088	−1·0	XS 2S03
(*c*)	−6·0	−1·5	−1·0266	$\frac{1}{4}$	$\frac{1}{2}$	4	−0·264	−3.0	XS 2S04
(*d*)	−4·0	−4·0	−2·7384	1	1	4	−0·352	−4·0	XS 2S07
(*e*)	−6·0	−6·0	−4·1076	1	1	4	−0·528	−6·0	XS 2S08
(*f*)	0·25	$\frac{1}{16}$	0·04278	$\frac{1}{4}$	$\frac{1}{2}$	4	0·011	$\frac{1}{8}$	XS 2009
(*g*)	0·5	$\frac{1}{8}$	0·08555	$\frac{1}{4}$	$\frac{1}{2}$	4	0·022	$\frac{1}{4}$	XS 2008
(*h*)	0·75	$\frac{3}{16}$	0·25665	$\frac{1}{4}$	$\frac{1}{2}$	4	0·033	$\frac{3}{8}$	XS 2003
(*i*)	1·5	$\frac{3}{8}$	0·12833	$\frac{1}{4}$	$\frac{1}{2}$	4	0·066	$\frac{3}{4}$	*XS* 2007
(*j*)	1·0	1·0	0·6846	1	1	−3	0·088	1·0	XS 2004
(*k*)	2·0	2·0	1·3692	1	1	−4	0·176	2·0	XS 2001
(*l*)	3·0	3·0	2·0538	1	1	−4	0·264	3·0	XS 2006
(*m*)	6·0	6·0	4·1076	1	1	−4	0·528	6·0	XS 200A

TABLE 1. Upper half-plane contour parameters for coaxial translating *V*-state interactions ($\omega_1 = 1{\cdot}0$, $\Gamma_1 = 0{\cdot}6846$, $V_1 = +0{\cdot}088$, $A_1 = 0{\cdot}6846$, $P_1 = 2{\cdot}985$; $A_2 = A_1$, $P_2 = P_1$ or $A_2 = 0{\cdot}1711$, $P_2 = 1{\cdot}493$). Here $\bar{x}_c = \bar{x}_2 - \bar{x}_1$, $V_2/V_1 = \Gamma_2\bar{y}_1/\Gamma_1\bar{y}_2$.

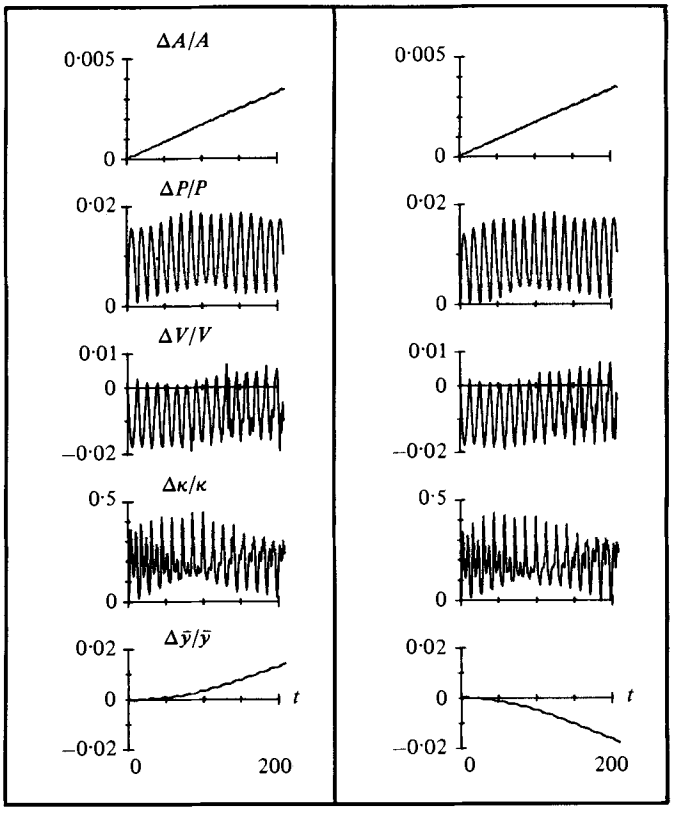

FIGURE 2. Diagnostics for the effects resulting from an asymmetric perturbation given to V-state H.

(iii) Since this perturbation increases the area of the upper contour by $(1/0{\cdot}9787)^2$, we rescale the linear dimensions by 0·9787 about the point (0, 0·15), that is,

$$x \to 0{\cdot}9787x, \quad y \to 0{\cdot}9787(y - 0{\cdot}15) + 0{\cdot}15.$$

The effects of this perturbation are given in the diagnostics of figure 2. A fifth figure is included that gives the relative change in the y-centroid position. In 200 units of time the V-state translates 20 units (about 20 V-state lengths) and we do not observe any instability. The initial perturbation introduces a nearly harmonic perimeter fluctuation of period 13·3 in both contours. This is also manifest in the relative velocity change and in the relative maximum-curvature change. (We also observe a second harmonic in this diagnostic.) The y-centroid motion results from the fact that the areas within the two contours agree initially to only four significant figures after the initial asymmetric perturbation is inserted. That is, since the areas differ, then the net circulations differ and the centroid of the state moves on a circle of very large radius.

3.4. *Head-On* ($\rightarrow \leftarrow$) *interactions* (*or* $\pm$ *on* $\mp$ *vorticity arrangements*)

Figure 3 (case *a*) is a composite that shows two approaching V-states with $\Gamma_2/\Gamma_1 = -1{\cdot}0$ and unlike area. They 'exchange' into an outgoing asymmetric nearly steady configuration, as discussed below. It is travelling in a north-easterly direction with a velocity intermediate between those of the incoming V-states. At $t = 0$ they are maximally separated ($\bar{x}_c(0) = 4{\cdot}0$) and the highest state shown is at $t = 60$. The

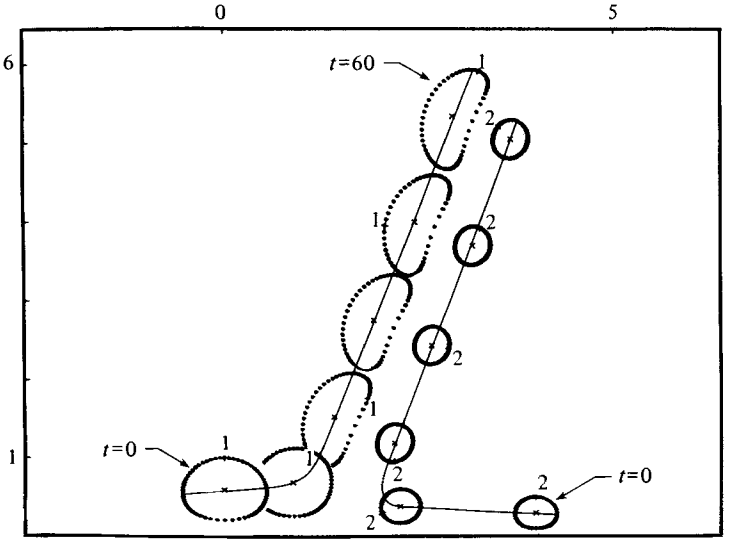

FIGURE 3. *V*-state 'exchange' in a head-on interaction: $\Gamma_2/\Gamma_1 = -1{\cdot}0$, case (*a*).

time increment between states is $\Delta t = 12$. The dots indicate the discretization used. The number of nodes on contours (1, 2) increased from (64, 66) at $t = 0$ to (77, 115) at $t = 60$. The ' × ' marks the centroids of the figures. The numbers on the contours label the same node and give one a feeling for its motion. Figure 11(*a*) repeats the trajectory diagram and figure 12(*a*) gives the phase-shift diagram.

Figure 4(*a*) contains four diagnostics for each of the contours. During the brief 'exchange' interval all quantities undergo abrupt changes. $(\Delta A/A)_1$ begins to increase at a more rapid rate because of its increased aspect ratio and the new region of negative curvature. The velocity of no. 1 increases and no. 2 decreases so as to conserve linear momentum. The new asymmetric state that has formed seems 'near' a *V*-state, for in $(\Delta P/P)_1$ and $(\Delta\kappa/\kappa)_1$ one sees small-amplitude oscillations about *new* steady values. (Note that the new steady perimeter is about 10% larger than the initial perimeter, whereas the perimeter change associated with the area change is 0·125%.

To examine more quantitatively the near-steady behaviour, we *remove* the lower-half-plane contours and *restart* the problem and run it for 50 additional time units. Diagnostics are given in figure 5. The larger contour exhibits a nearly harmonic perimeter fluctuation of 0·5% amplitude, an effect also manifest in the other diagnostics. Also, the 5% peak $\Delta\kappa/\kappa$ fluctuation is consistent with a very small perturbation from a steady configuration.

Case (*b*) given in figure 6(*b*) is the result of changing the circulation ratio Γ_2/Γ_1 to $-0{\cdot}5$. The approaching *V*-states undergo a complicated interaction where no. 1 passes *below* no. 2 as shown in the trajectory diagram of figure 11(*b*) and the 'phase-shift' diagram of figure (12*b*).

A complete set of diagnostics is shown in figure 4(*b*). $\Delta P/P$ and $\Delta V/V$ are almost exactly symmetric about a point in time. The change in sign in $(\Delta P/P)_2$ (see ←) toward the end of the run is probably due to the numerically induced area change seen in $(\Delta A/A)_2$.

Case (*c*), given in figure 6(*c*) is the result of changing the circulation ratio Γ_2/Γ_1 to $-1{\cdot}5$. During the interaction, no. 1 passes *above* no. 2, as shown in figure 11(*c*), and no. 1 is left in an excited (distorted) state as it translates to the right. The diagnostics

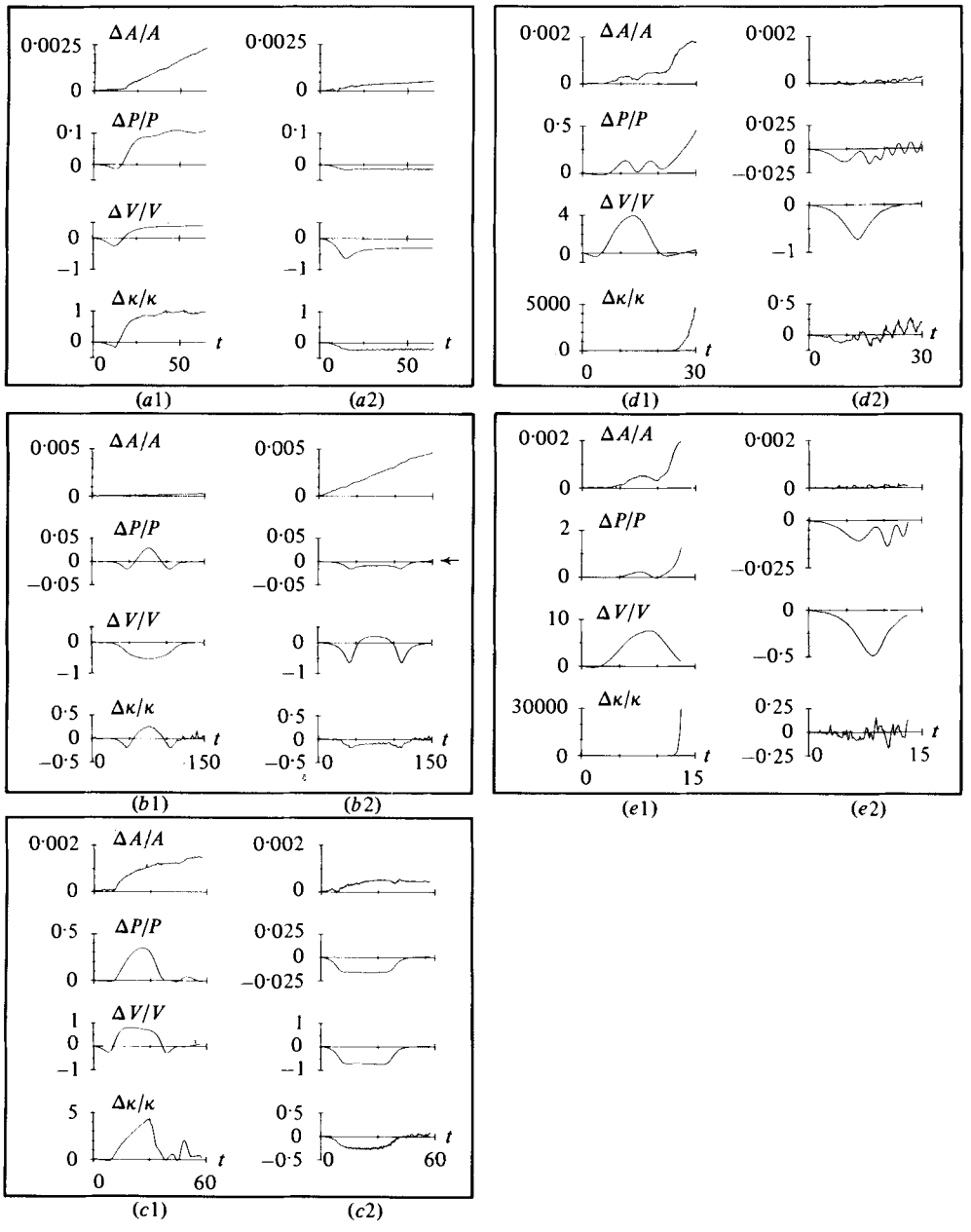

FIGURE 4. Diagnostics for head-on interactions: area change $\Delta A/A$; perimeter change $\Delta P/P$; velocity change $\Delta V/V$; maximum-curvature change $\Delta\kappa/\kappa$.

given in figure 4 (c) show a stronger and less symmetric interaction than obtained in case (*b*), and contour 1 is left with small perimeter and curvature fluctuations. Figure 12 (*c*) shows the phase-shift diagram, where no. 1 is accelerated and no. 2 is decelerated through the interaction, the reverse of the processes that occurs in case *b*.

Figures 6 (*d*) and (*e*) give head-on cases where no. 1 and no. 2 have the same area (no. 2 has been increased by a factor of 4·0) and the circulation ratios are $-4{\cdot}0$ and $-6{\cdot}0$, respectively. This causes no. 1 to loop above no. 2 (as shown in figures 11 *d*, *e*), consistent with case (*c*). Case (*d*) shows a 'weak' tendency to break, and case (*e*) shows

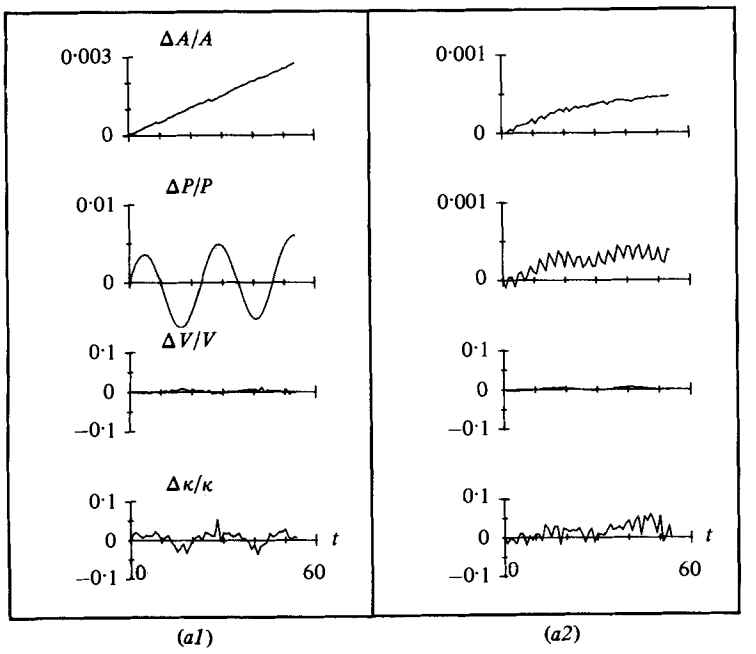

FIGURE 5. Diagnostics for the continuation of case (*a*).

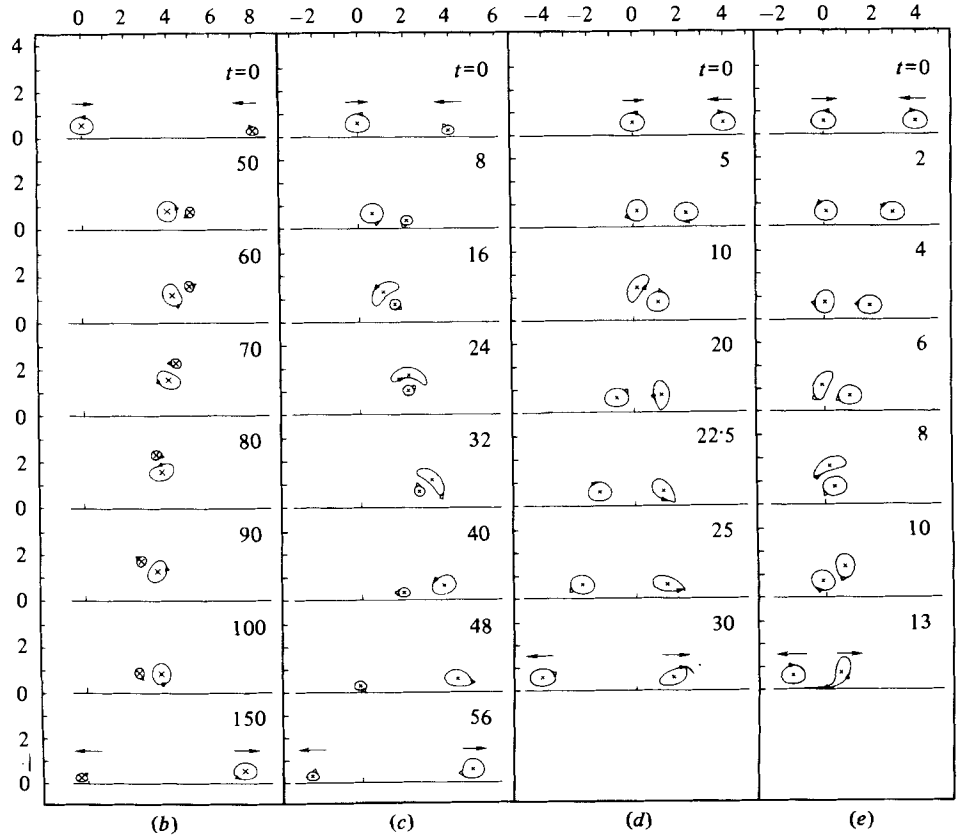

FIGURE 6. Head-on interactions (letters refer to cases in table 1); (*b*) $\Gamma_2/\Gamma_1 = -\frac{1}{2}$; (*c*) $\Gamma_2/\Gamma_1 = -1{\cdot}5$; (*d*) $\Gamma_2/\Gamma_1 = -4{\cdot}0$; (*e*) $\Gamma_2/\Gamma_1 = -6{\cdot}0$.

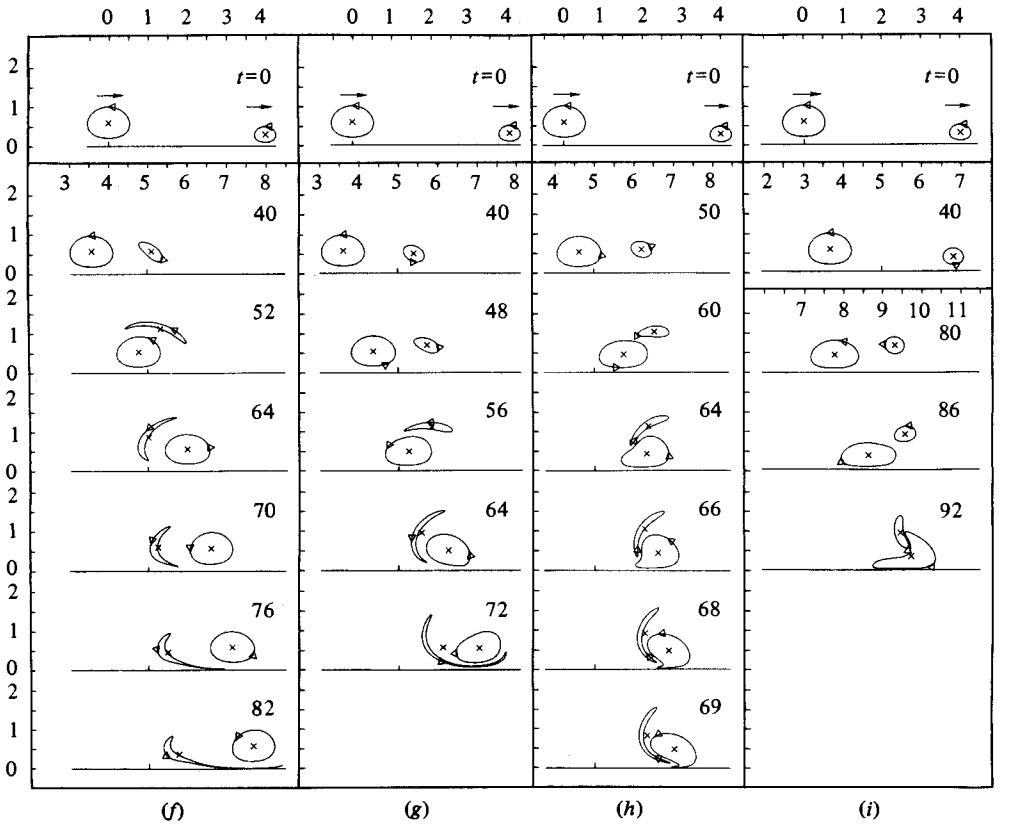

FIGURE 7. Head–tail interactions (letters refer to cases in table 1): (*f*) $\Gamma_2/\Gamma_1 = \frac{1}{16}$; (*g*) $\Gamma_2/\Gamma_1 = \frac{1}{8}$; (*h*) $\Gamma_2/\Gamma_1 = \frac{3}{16}$; (*i*) $\Gamma_2/\Gamma_1 = \frac{3}{8}$.

a stronger interaction and breaking occurs earlier. This is seen in the *earlier* and *larger* perimeter growth in case (*e*) compared with case (*d*). Note that $(\Delta P/P)_2$ is 'ringing' after the interaction, and the oscillation is in-phase with $\Delta\kappa/\kappa$. It is reasonable to expect that a piece of no. 1 would have elongated around no. 2, before it escaped to the right if we have examined a case where the circulation ratio was made $> 6{\cdot}0$.

3.5. *Head–tail* ($\rightarrow\ \rightarrow$) *interactions* (*or* $\pm$ *on* $\pm$ *vorticity arrangements*)

Figures 7 (*f–i*) show four *head–tail* cases, where the area ratio is 1 : 4 and the circulation ratios Γ_2/Γ_1 are $(\frac{1}{16}, \frac{1}{8}, \frac{3}{16}, \frac{3}{8})$. As one increases the circulation ratio towards unity, the 'wrap-around' tendency becomes stronger. Finally, capture is observed in (*i*). Diagnostics $\Delta P/P$ and $\Delta V/V$ are given in figure 8. The tendency towards capture is shown in $(\Delta P/P)_1$, whose final amplitude increased monotonically (from *f–i*), and in $(\Delta V/V)_2$, whose value is increasing at the end of the run (cases (*h*) and (*i*), see ↑).

Figures 9 (*j–m*) show four head–tail cases where the area ratio is 1 : 1 and the circulation ratios Γ_2/Γ_1 are 1·0, 2·0, 3·0 and 6·0. Since cases (*i*)–(*k*) bear a resemblance, we conclude that *if the areas of V-states are sufficiently close, head–tail interactions in the range* $\frac{3}{8} < \Gamma_1/\Gamma_2 < \frac{8}{3}$ *lead to 'capture' or 'merger' of like-signed vorticity regions.* If more runs were made, and some dissipative regularization introduced, we would undoubtedly sharpen the boundaries of Γ_2/Γ_1 ratios.

There is less of a tendency towards 'capture' as the circulation ratio increases beyond 2·0. However, both contours develop regions of high curvature as shown for

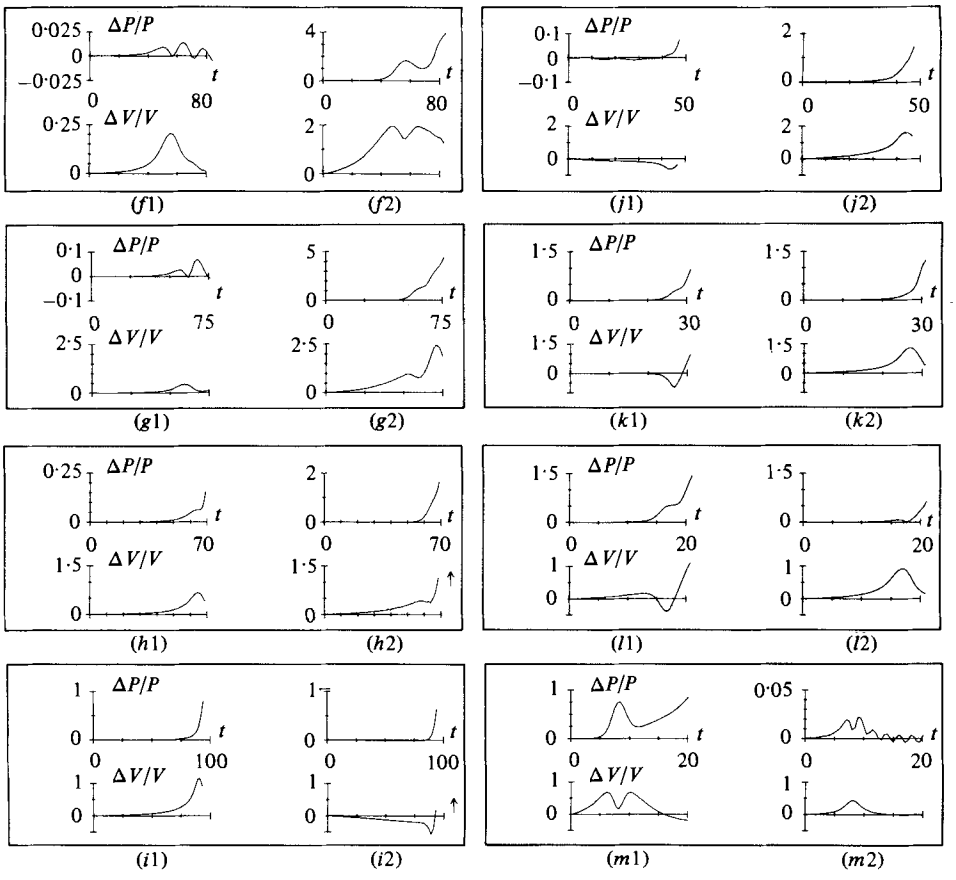

FIGURE 8. Diagnostics for head–tail interactions: $\Delta P/P$ and $\Delta V/V$.

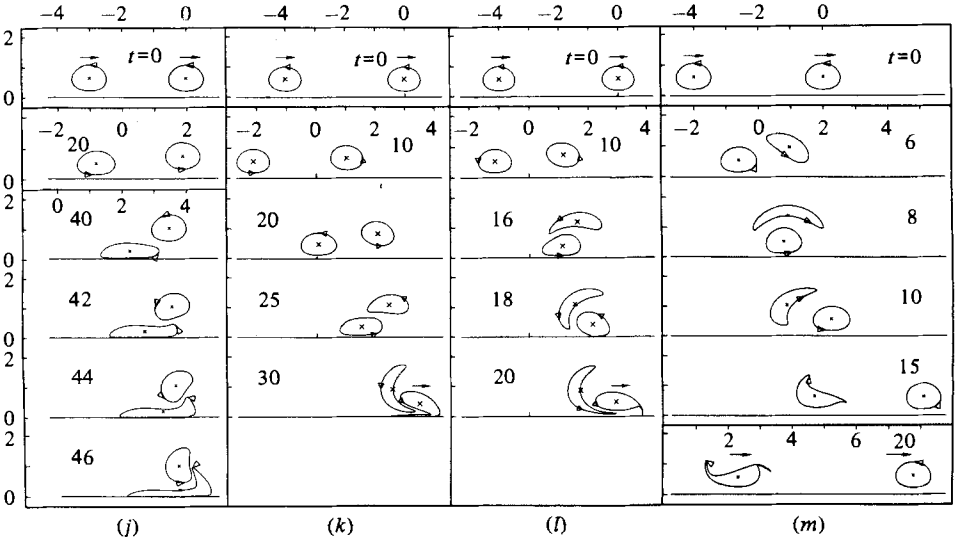

FIGURE 9. Head–tail interactions: (*j*) $\Gamma_2/\Gamma_1 = 1{\cdot}0$; (*k*) $\Gamma_2/\Gamma_1 = 2{\cdot}0$; (*l*) $\Gamma_2/\Gamma_1 = 3{\cdot}0$; (*m*) $\Gamma_2/\Gamma_1 = 6{\cdot}0$.

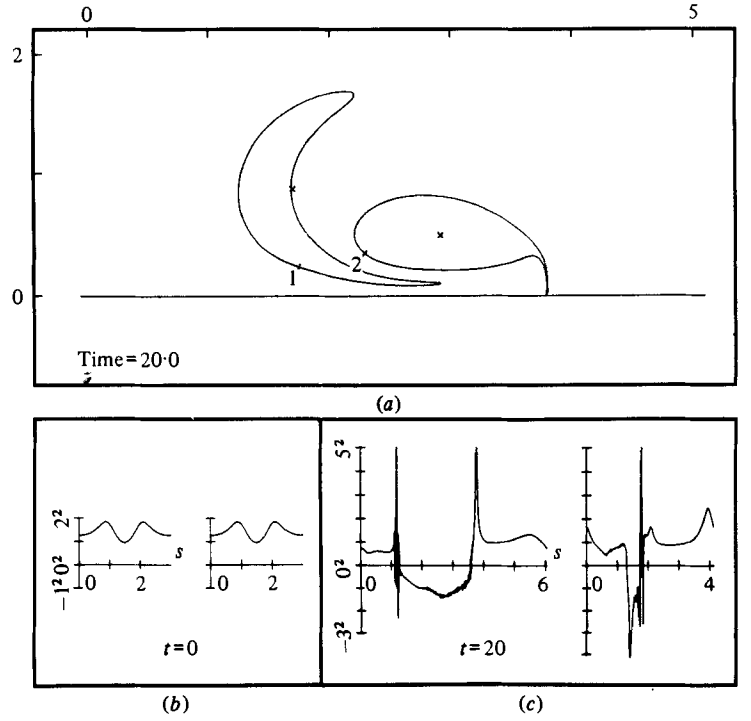

FIGURE 10. Upper-half-plane V-states, case (l), $t = 20$. Initial and final curvatures for case (l). (The curvature scales have a geometric variation and are clipped at $\pm 5^2$.)

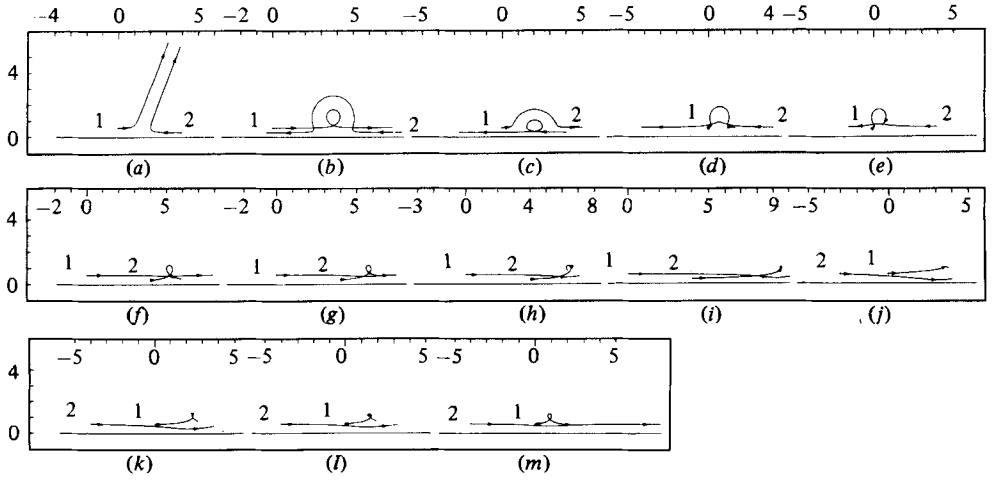

FIGURE 11. Trajectory diagrams ($\bar{x}(t)$, $\bar{y}(t)$). (All space scales are identical.)

case (l) in figure 10. The circumferences have increased from (2·985, 2·985) at $t = 0$ to (6·033, 4·113) at $t = 20$, and the number of nodes has increased from (64, 64) to (252, 157) respectively.

4. Conclusions

The panorama of results shows clearly the qualitative effects of interaction symmetry (i.e. head-on *vs.* head–tail), internal degrees of freedom (or self-consistent contour interactions), and V-state size on the nature of coaxial V-state interactions. Head–tail interactions show a greater tendency to break (or cascade 'enstrophy' to

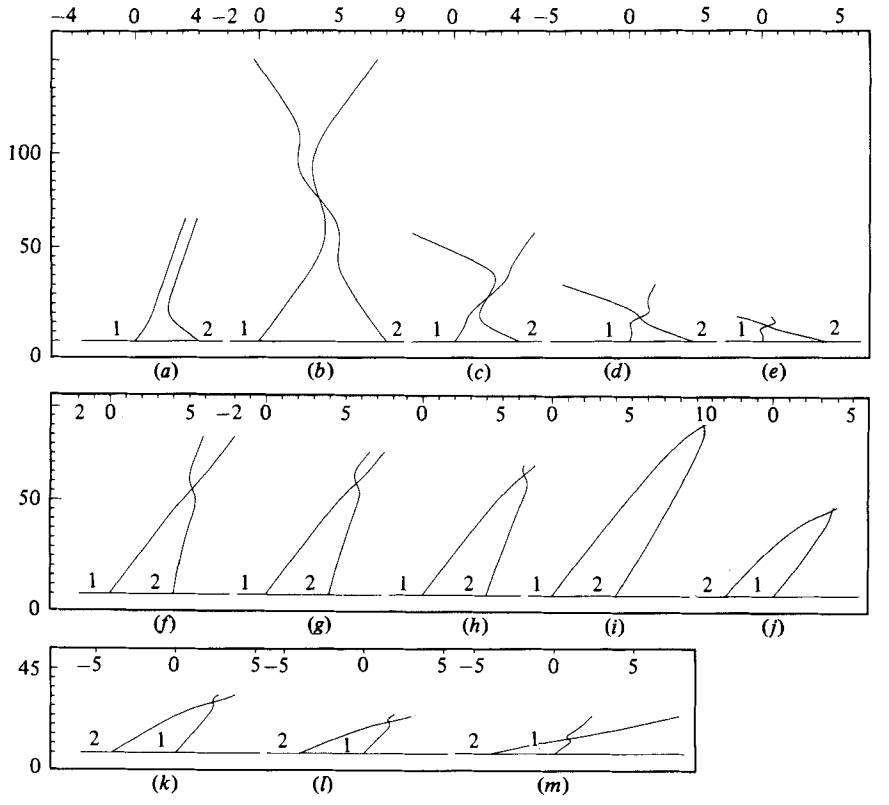

FIGURE 12. Phase-shift diagrams ($\bar{x}(t)$, t). (Space and time scales are identical for all figures.)

higher wavenumbers), probably because of the nature of flow fields produced by dipolar $\pm$ on $\pm$ vortex distributions. Vortex regions of larger spatial extent show a greater tendency to break. A quantitative understanding of these phenomena and their dependence on aspect ratio and non-coaxiality await more detailed analytical and computational studies. For example, if the effective radii of the interacting V-states are small compared with their distance of vertical separation, then the contours are weakly perturbed. Thus, it is possible that we can obtain essential features of such an interaction by initially replacing each V-state by two (Love 1894) or more point vortices. However, for close interactions of physically realistic vorticity distributions, we will require V-states containing several *nested* contours. To avoid the computational burden associated with breaking and the development of regions of high curvature at long times, we are required to introduce dissipative regularization (Zabusky & Overman 1982) and contour topology changes. The former process realistically mimics viscous smoothing. In the latter processes, we will cut and rejoin the same contour if regions approach or cut and eliminate regions of different contours if these regions approach too closely.

The algorithm development work was supported by the Office of Naval Research, contract N00014-77-C-0520, Task NR 062 583. The applications to head-on and head-tail interactions was supported by the Army Research Office, contract DAAG-29-80-K-0072. The original simulations of cases (*a*)–(*l*) as shown in figures 2, 4, 5 and 7 were performed on the CRAY-1 computer at the National Center for Atmospheric Research (supported by the National Science Foundation) through a computer-time grant.

state	$y_{\min}$	$\bar{y}$	A	P	V	V/V^*
A	0·9	0·9499	0·7839	0·4141	−0·6567	1·000
B	0·8	0·8997	0·3143	0·7294	−0·2773	1·000
C	0·7	0·8495	0·7136	1·049	−0·6681	1·000
D	0·6	0·7993	0·1290	1·376	−0·1278	0·996
E	0·5	0·7487	0·2071	1·718	−0·2193	0·996
F	0·4	0·6975	0·3116	2·088	−0·3535	0·995
G	0·3	0·6446	0·4565	2·519	−0·5552	0·985
H	0·2	0·5873	0·6816	3·098	−0·8819	0·955
I	0·1	0·5171	0·1133	4·163	−0·1486	0·852
J	0·05	0·4729	0·1592	5·158	−0·1969	0·735
K	0·01	0·4296	0·2225	6·731	−0·2446	0·594

TABLE 2. Symmetric dipolar translating V-states

Appendix A. Properties of symmetric dipolar translating V-states

Table 2 presents properties of the translating V-states. These were obtained by solving a discretized form of (8) by the method of Pierrehumbert. N corresponds to the case letters, some of which are shown in figure 1. We used state H in all simulations presented in this paper. The states lie in the range $y_{\min} \leqslant y \leqslant 1{\cdot}0$, and $\bar{y}$ is the distance from the x-axis to the upper-half-plane centroid. A is the area and P is the perimeter of the upper-half-plane contour. V is the translating velocity of the V-state and V/V^* is a normalized speed, where V^* is given in (5).

Appendix B. The improved contour-dynamical algorithm

If we perform the integration in (4) over *straight-line* segments joining each node on a contour we obtain (9), where

$$\Delta u_{m,n} = \frac{h_n}{2\pi}\Big[(1+A_{mn})\ln r_{m,n+1} - A_{mn}\ln r_{m,n} - 1 + B_{mn}\arctan\frac{2B_{mn}}{C_{mn}} + \pi|B_{mn}|H(-C_{mn})\Big] \quad (B\,1)$$

Here $r_{m,n}$ is the straight-line distance between nodes m and n (we have suppressed the subscript i that labels the contours),

$$A_{mn} = \frac{(x_n - x_m)\,(x_{n+1} - x_n) + (y_n - y_m)(y_{n+1} - y_n)}{h_n^2}, \quad (B\,2)$$

$$B_{mn} = \frac{(x_n - x_m)\,(y_{n+1} - y_n) - (y_n - y_m)\,(x_{n+1} - x_n)}{h_n^2}, \quad (B\,3)$$

$$C_{mn} = \frac{r_{m,n}^2 + r_{n,m+1}^2}{h_n^2} - 1, \quad (B\,4)$$

and H is the Heaviside step function, i.e.

$$H(z) = \begin{cases} 1 & (z \geqslant 0), \\ 0 & (z < 0). \end{cases}$$

If $n = m$, (B 1) simplifies to

$$\Delta u_{m,m} = \frac{1}{2\pi}[\ln r_{m,m+1} - 1], \quad (B\,5)$$

since $A_{mm} = B_{mm} = 0$, while if $n = m-1$

$$\Delta u_{m,\,m-1} = \frac{1}{2\pi}[\ln r_{m,\,m-1} - 1], \tag{B 6}$$

since $A_{m,\,m-1} = -1$ and $B_{m,\,m-1} = 0$.

Equation (B 1) differs from the previously given value (equation (18) of McWilliams 1980) in the last term. This term appears only when $C_n < 0$ or, equivalently, if the angle between the lines from node m to node n *and* from node m to node $n+1$ is $\geqslant \frac{1}{2}\pi$. This may occur if a contour breaks and forms filaments whose sides approach or if two different contours approach close to one another in a merger, because the node-insertion-and-removal algorithm maintains $h_n \geqslant h_{\min}$, an *a priori* prescribed value.

The velocities in (9) are used to move the contour nodes $(x_n,\ y_n)$ with an Euler-predictor and a trapezoidal-corrector algorithm. The time step Δt is determined by the maximum change in area (or angular momentum) to be allowed per unit time. (Since we are solving a Lagrangian system of equations, we do not have a Courant condition to determine the time step.) In all the runs shown here the relative area change per step is $\Delta A/A = 0{\cdot}84375 \times 10^{-6}$ and Δt is readjusted every 20 time steps. We find that $0{\cdot}015 \leqslant \Delta t \leqslant 0{\cdot}02$ for all the runs.

In the *improved* node-insertion-and-removal algorithm we insert and remove nodes using both local (Zabusky *et al.* 1979) and global adaptive methods. Locally, we attempt to set the internodal distance h_k to $c_1|\kappa_k|^{-1}$, which is inversely proportional to the local curvature, but we require it to satisfy two constraints:

$$h^{(g)}_{\max} \geqslant h_k \geqslant h_{\min}, \tag{B 7}$$

$$(1-r)\,h_{k-1} \leqslant h_k \leqslant (1+r)\,h_{k-1}. \tag{B 8}$$

In all the runs $c_1 = 0{\cdot}1$ (which places $\sim 20\pi$ nodes on a circle of unit radius), $h_{\min} = 0{\cdot}01$ and $r = 0{\cdot}3$. Globally, we choose $h^{(g)}_{\max}$ to take into account the possibility that one part of a contour may approach another part or that two contours may approach each other. This is done by setting

$$h^{(g)}_{\max} = \max\,[\min\,\{h_{\max}, c_2\,d_{\min}\}, h_{\min}] \tag{B 9}$$

where $d_{\min}$, obtained by a search algorithm, is the minimum distance from node k to a point on a neighbouring contour or a 'non-adjacent' point on the same contour. Usually $h^{(g)}_{\max}$ will be the minimum of $h_{\max}$, the maximum allowed distance between nodes, or $c_2 d_{\min}$ (in all our runs $h_{\max} = 0{\cdot}20$ and $c_2 = 0{\cdot}50$).

REFERENCES

Deem, G. S. & Zabusky, N. J. 1978*a* Stationary *V*-states: interactions, recurrence and breaking. *Phys. Rev. Lett.* **40**, 859.

Deem, G. S. & Zabusky, N. J. 1978*b* Stationary '*V*-states': interactions, recurrence and breaking. In *Solitons in Action* (ed. K. Lonngren & A. Scott), pp. 277–293, Academic.

Flierl, G. R., Larichev, V. D., McWilliams, J. C. & Reznick, G. M. 1980 The dynamics of baroclinic and barotropic solitary eddies. *Dyn. Atmos. Oceans.* **5**, 1–41.

Love, A. E. H. 1894 On the motion of paired vortices with a common axis. *Proc. Lond. Math. Soc.* **25**, 185.

McWilliams, J. C. 1980 An application of equivalent modons to atmospheric blocking. *Dyn. Atmos. Oceans* **4**, 43–46.

McWilliams, J. C. & Zabusky, N. J. 1982 Interactions of isolated vortices. I. Modons colliding with modons. *Geophys. Astrophys. Fluid Dyn.* **19**, 207–227.

MAKHANKOV, V. G. 1980 Computer experiments in soliton theory. *Comp. Phys. Commun.* **21**, 1–49.

OVERMAN II, E. A. & ZABUSKY, N. J. 1982 Evolution and merger of isolated vortex structures. *Phys. Fluids* **25**, 1297–1306.

PIERREHUMBERT, R. T. 1980 A family of steady translating vortex pairs with distributed vorticity. *J. Fluid Mech.* **99**, 129–144.

SIMONOV, YU, A. & TJON, J. A. 1980 Inelastic effects in classical field-theoretical models with confinement. *Ann. Phys. (N.Y.)* **129**, 110–130.

WU, H. M., OVERMAN II, E. A. & ZABUSKY, N. J. 1982 Steady-state solutions of the Euler equations in two dimensions. Rotating and translating V-states with limiting cases. *Preprint, I.C.M.A., University of Pittsburgh.* Submitted to *J. Comp. Phys.*

ZABUSKY, N. J. 1981 Computational synergetics and mathematical innovation. *J. Comp. Phys.* **43**, 195–249.

ZABUSKY, N. J., HUGHES, M. H. & ROBERTS, K. V. 1979 Contour dynamics for the Euler equations in two dimensions. *J. Comp. Phys.* **30**, 96–106.

ZABUSKY, N. J. & OVERMAN II, E. A. 1982 Regularization of contour dynamical algorithms. *J. Comp. Phys.* (to be published).